Sensors and Materials, Vol. 37, No. 5 (2025) 2005–2011
MYU Tokyo

S & M 4037

Feasibility Study of Thallium Bromide Detectors for Boron Neutron Capture Therapy Applications

Keitaro Hitomi,[1*] Mitsuhiro Nogami,[1] Kenichi Watanabe,[2]
Nishiki Matsubayashi,[3] and Hiroki Tanaka[3]

[1]Department of Quantum Science and Energy Engineering, Graduate School of Engineering, Tohoku University, 6-6-01-2 Aza-Aoba, Aramaki, Aoba-ku, Sendai 980-8579, Japan
[2]Department of Applied Quantum Physics and Nuclear Engineering, Kyushu University, 744 Motooka, Nishi-ku, Fukuoka, Japan
[3]Institute for Integrated Radiation and Nuclear Science, Kyoto University, 2 Asashiro-Nishi, Kumatori-cho, Sennan-gun, Osaka 590-0494 Japan

(Received February 28, 2025; accepted April 23, 2025)

Keywords: thallium bromide (TlBr), boron neutron capture therapy (BNCT), gamma-ray detector, compound semiconductor, prompt gamma ray detection

A thallium bromide (TlBr) detector with four-channel readout electrodes was fabricated from a crystal grown by the traveling molten zone method from a zone-purified material for boron neutron capture therapy applications. The detector crystal dimensions were 12 × 12 × 10 mm^3. The detector had four circular anodes of 2 mm diameter. The detector exhibited energy resolutions sufficient to resolve 478 keV gamma rays from 511 keV gamma rays. A prompt gamma-ray detection system was constructed using the TlBr detector and a tungsten collimator. A mouse phantom with a tumor sphere containing 1475 ppm ^{10}B was irradiated with thermal neutrons. The ^{10}B distribution was imaged successfully with the TlBr detector system. The detector system exhibited a linear relationship between the counts for 478 keV and the ^{10}B concentration in the range of 0–5000 ppm.

1. Introduction

Boron neutron capture therapy (BNCT) is a cancer therapy using $^{10}B(n, \alpha)^7Li$ reactions. The boron dose can be estimated by detecting the prompt gamma rays of 478 keV resulting from the reactions. Scintillation and semiconductor detectors including $LaBr_3$, $Ce:Gd_3Al_2Ga_3O_{12}$ (GAGG), Ge, CdTe, and $CdZn_xTe_{1-x}$ (CZT) detectors and Si/CdTe Compton cameras have been studied for BNCT applications.[1–12] Positron annihilation gamma rays of 511 keV and 2.22 MeV gamma rays produced by $^1H(n, \gamma)^2H$ reactions are significant sources of background for detecting 478 keV gamma rays during BNCT. The gamma-ray detectors for BNCT applications should have sufficient energy resolutions to resolve 478 keV gamma rays from 511 keV gamma rays. In addition to the energy resolutions, high peak efficiencies are required for the detectors

*Corresponding author: e-mail: keitaro.hitomi.d4@tohoku.ac.jp
https://doi.org/10.18494/SAM5613
Part of this paper was published in the Report on the Research Achievements of the Grants-in-Aid for Scientific Research (JSPS KAKENHI Grant No. JP20H00656) (in Japanese).

because the 478 keV gamma rays are overlapped on the Compton continuum associated with the background gamma rays.

Thallium bromide is an attractive semiconductor material for constructing gamma ray detectors for BNCT applications because of its high photon stopping power originating from its high atomic numbers (81 and 35) and high density (7.56 g/cm^3). The wide bandgap energy of 2.68 eV for the TlBr crystal allows the detector to operate at room temperature. Energy resolutions of 1.5–1.8% full width at half-maximum (FWHM) for 662 keV gamma rays were obtained from a pixelated TlBr detector at room temperature.[13] Gamma ray detectors using TlBr crystals have been studied by various researchers, as described in a review article.[14] A Monte Carlo simulation study was carried out for a multiple-scattering Compton camera based on TlBr detectors for BNCT.[15] The practical applications of TlBr detectors, however, have been limited because of the instability of their performance. Recently, significant improvements in the stability of TlBr detectors with Tl electrodes have been achieved, demonstrating 1000 h of stable operation at room temperature.[16]

Because it has higher photon stopping power than $LaBr_3$, GAGG, Si, Ge, CdTe, and CZT for 478 keV gamma rays and higher energy resolution than the $LaBr_3$ and GAGG scintillators, TlBr is a promising detector material for the construction of detector systems for BNCT applications.

In this study, the ^{10}B distribution in a mouse phantom irradiated with a thermal neutron beam at the Kyoto University Research Reactor (KUR) was obtained by detecting 478 keV gamma rays with a gamma-ray detector system consisting of a four-channel TlBr detector with a tungsten collimator.

2. Experiments

A gamma-ray detector system for measuring ^{10}B distributions was constructed using a TlBr detector and a tungsten collimator. The arrangement of the collimator and the detector is shown in Fig. 1(a). The TlBr detector was placed in a shield box made of 5-mm-thick aluminum. The tungsten collimator was placed close to the outside of the aluminum box. The collimator was fabricated by connecting three tungsten blocks with the dimensions of 12 × 25 × 25 mm^3. The 12 × 25 mm^2 face of the center block had six holes of 2 mm diameter, as shown in Fig. 1(b). The TlBr detector was fabricated from the crystal grown by the traveling molten zone method from a zone-purified material. The grown crystal was cut into cubes, and the two opposing surfaces were polished mechanically for electrode deposition. The detector crystal has the dimensions of 12 × 12 × 10 mm^3. The cathode and anode of the detector were constructed by the vacuum evaporation of Tl on the 12 × 12 mm^2 polished surfaces of the crystal. The employment of Tl as the electrode material improves the stability of TlBr detectors at room temperature.[17,18] A planar electrode of 10 × 10 mm^2 area was formed on the cathode surface. The anode consisted of four circular electrodes of 2 mm diameter and surrounding electrodes, as shown in Fig. 1(c). Thin gold wires were attached to the electrodes with carbon paste for signal readout. The detector was coated with epoxy resin to prevent the oxidation of the Tl electrodes. The detailed detector fabrication process of the stable TlBr detectors employed in this study has been described in the literature.[16]

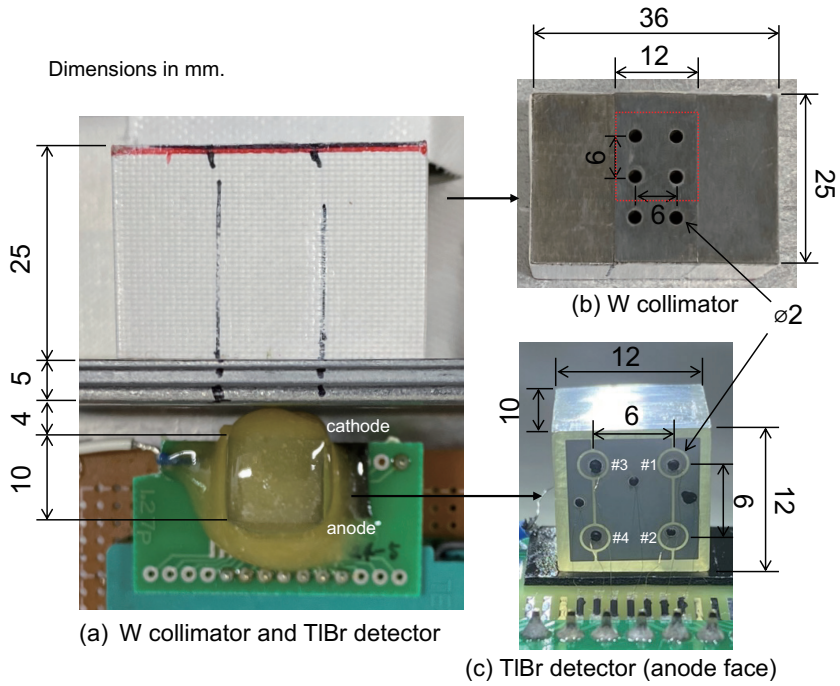

Fig. 1. (Color online) (a) Arrangement of W collimator and TlBr detector. During the measurements, an electrical insulator made of thin sheets of paper was placed between the cathode side of the detector and the Al box. (b) W collimator. The four holes within the red dotted square were used for the detector. (c) TlBr detector before epoxy coating. The gap between the circular electrodes and the surrounding electrodes was 0.2 mm.

The four anodes and the cathode of the TlBr detector were connected to a four-channel charge-sensitive preamplifier (Clear Pulse 5005H) and to a charge-sensitive preamplifier (Clear Pulse 580K), respectively. The cathode was biased at 1000 V. The anodes and surrounding electrodes were maintained at ground potential. The output signals from the preamplifiers were recorded with a digitizer (Clear Pulse 80442) with the vertical resolution of 14 bits and the sampling rate of 10 MS/s. A digital trapezoidal filter with the rise time of 18 μs and the flat top time of 4 μs was applied to the waveforms from the detector to obtain the pulse height spectra. The gamma-ray interaction depth in the detector was determined using the cathode-to-anode signal (C/A) ratio.[19,20] The near-cathode events were selected on the basis of the C/A ratio to obtain the anode spectra with good energy resolutions. Multi-electrode hit events in the detector, which exhibit a C/A ratio greater than 1, were rejected to improve the peak-to-Compton and peak-to-escape ratios.

Mouse phantoms with a 1-cm-diameter sphere simulating the tumor region were fabricated with a 3D printer. The body of the mouse phantom and the tumor sphere contained water and boric acid solution, respectively. The tumor sphere of the mouse phantom was irradiated with an 18×15 mm^2 thermal neutron beam with the flux of 2×10^6 n/cm^2/s from the E3 neutron guide tube of KUR (5 MW). Prompt gamma rays from the phantom during the neutron irradiation were measured with the TlBr gamma-ray detector system, as shown in Fig. 2. To obtain a ^{10}B distribution for a mouse phantom with a tumor sphere containing 1475 ppm ^{10}B, a 24×24 mm^2

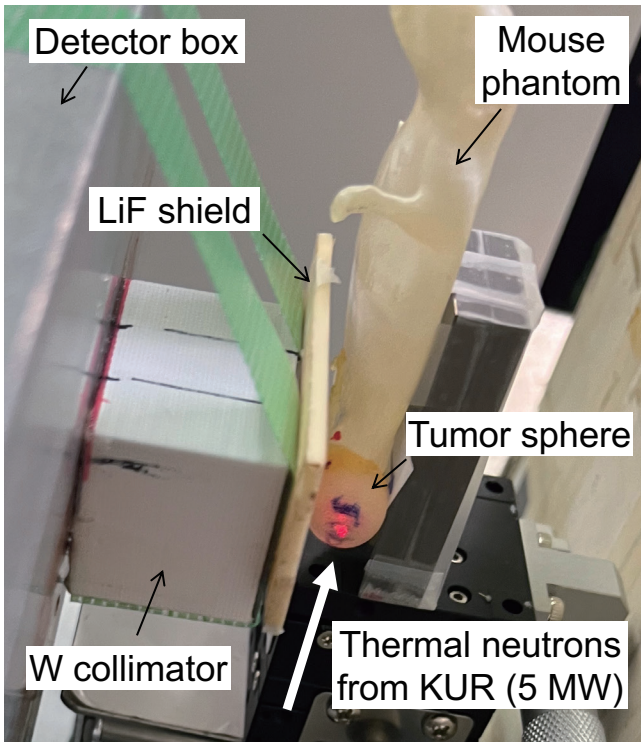

Fig. 2. (Color online) Experimental setup for prompt gamma ray measurements. A thermal neutron shield made of ^{6}Li-enriched (95%) LiF ceramic of 3 mm thickness was placed between the phantom and the collimator. The tumor sphere was irradiated with an 18 × 15 mm^2 thermal neutron beam with the flux of 2 × 10^6 n/cm^2/s. The red laser indicated the irradiation center. The distance between the collimator and the center of the tumor sphere was 8 mm (3 mm for the LiF ceramic and 5 mm for the radius of the tumor sphere).

region over the tumor was divided into four sections, and the measurements for each 12 × 12 mm^2 section were performed sequentially by moving the TlBr detector. Each measurement was performed for 40 min in real time. The linearity between the counts for 478 keV and the ^{10}B concentration was evaluated by measuring the prompt gamma rays from the phantoms with the tumor sphere containing 0, 500, 1475, and 5000 ppm ^{10}B. The spectrum acquisition time for each ^{10}B concentration was 40 min in real time.

3. Results and Discussion

Gamma-ray spectra obtained from the mouse phantom with a tumor sphere with 1475 ppm ^{10}B irradiated with thermal neutrons are shown in Fig. 3(a). Full-energy peaks for 478 and 511 keV were observed in the spectra, demonstrating the energy resolutions of the detector sufficient to resolve the peaks. The significant peak at 478 keV was obtained from detector channel #3 close to the tumor sphere (column 2, row 2, starting from the bottom right of the figure). The FWHM of the peak was measured to be approximately 4%.

The distribution of region of interest (ROI) counts for 478 keV gamma rays obtained from the experiment is shown in Fig. 3(b), superimposed on the mouse phantom at approximately the

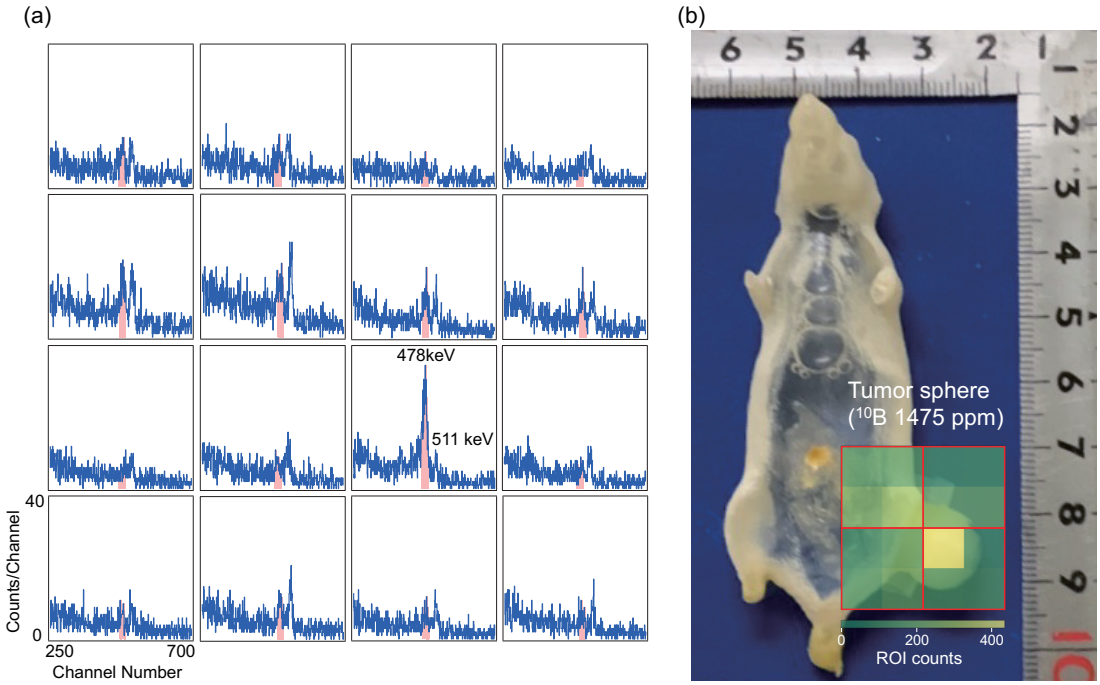

Fig. 3. (Color online) (a) Prompt gamma-ray spectra for a mouse phantom with a tumor containing 1475 ppm ^{10}B irradiated with thermal neutrons obtained from a four-channel TlBr detector. The 24 × 24 mm^2 region over the tumor was divided into four sections, and the measurements for each 12 × 12 mm^2 section were performed sequentially by moving the TlBr detector. (b) Distribution of ROI counts for 478 keV gamma rays superimposed on the mouse phantom at approximately the measurement position. The ROI count was defined as the counts within ±2% of the peak position for 478 keV (the shaded areas). The red squares indicate the detector position for each measurement.

measurement position. By assuming the same energy resolution for all anodes, the ROI count was defined as the counts within ±2% of the peak position for 478 keV. As can be seen from the figure, the high ROI count region well matched the position of the tumor sphere containing ^{10}B of 1475 ppm. The position resolution of the detector system was mainly determined by the collimator and the electrode designs. Experimental determination of the position resolution using a point source is necessary and will be a task for a future study. The field of view (FOV) of the TlBr detector system was limited because of the small detector area. Increasing the area of the TlBr detector is necessary for increasing the FOV.

In a previous study, a two-dimensional count distribution of 478 keV prompt gamma rays from a 50 ppm ^{10}B sample irradiated with a thermal neutron beam with the flux of 4.0 × 10^5 n/cm^2/s was obtained from a prompt gamma-ray imaging detector using a $LaBr_3$(Ce) scintillator without a collimator.(1) Characterization of the TlBr detector system for lower ^{10}B concentrations is necessary in order to consider the possibility of using the detector system for practical BNCT applications.

Figure 4 shows gamma ray spectra obtained from channel #3 of the detector placed close to the tumor sphere [corresponding to the position for column 2, row 2, starting from the bottom right of Fig. 3(a)] irradiated with thermal neutrons. The concentration of ^{10}B in the tumor sphere

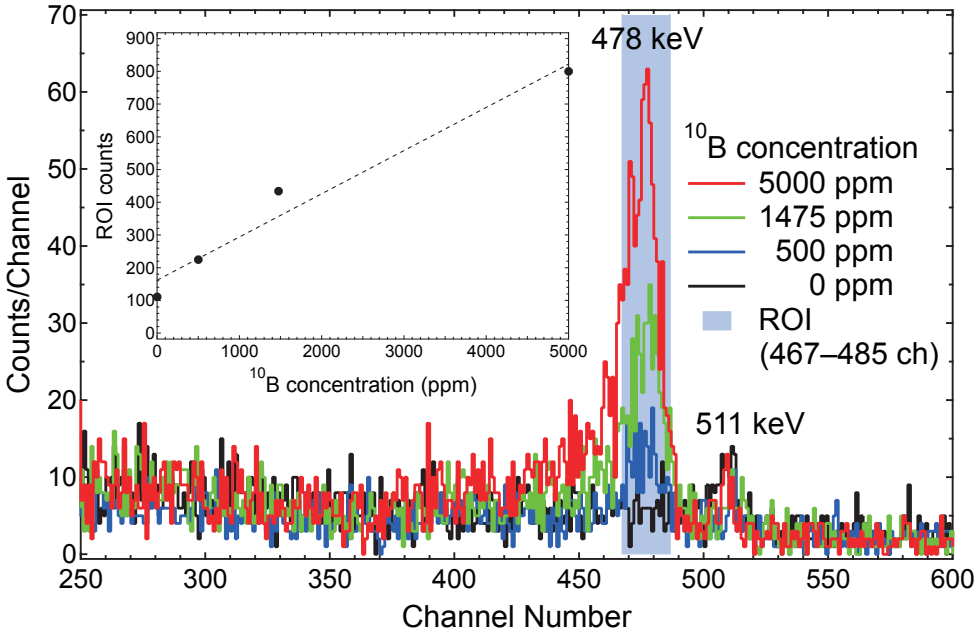

Fig. 4. (Color online) Prompt gamma-ray spectra obtained from channel #3 of the TlBr detector placed close to a tumor sphere of a mouse phantom irradiated with thermal neutrons. The concentration of ^{10}B in the tumor sphere was varied as 0, 500, 1475, and 5000 ppm. The inset shows the ROI counts for 478 keV gamma rays as a function of ^{10}B concentration.

was varied as 0, 500, 1475, and 5000 ppm. The ROI counts for 478 keV gamma rays as a function of the ^{10}B concentration are shown in the inset of Fig. 4. An almost linear relationship between the ^{10}B concentration and the ROI counts was obtained from the TlBr detector. Improving the position accuracy between the detector and the tumor spheres for the different ^{10}B concentrations and increasing the ROI counts are topics for future study.

4. Conclusions

A TlBr gamma-ray detector system was constructed for measuring ^{10}B distributions for BNCT applications. The TlBr detector exhibited a spectroscopic performance capable of resolving gamma peaks with the energies of 478 and 511 keV. Prompt gamma rays from a mouse phantom irradiated with thermal neutrons were measured with the TlBr detector system. An accumulation of ^{10}B in the tumor region was imaged successfully with the detector system. The TlBr detector exhibited a linear response between the ROI counts for 478 keV gamma rays and the ^{10}B concentrations. Future study should focus on increasing the area of the detector for practical applications.

Acknowledgments

This work was supported by JSPS KAKENHI Grant No. JP20H00656.

References

1 K. Okazaki, H. Tanaka, T. Takata, S. Kawabata, K. Akabori, and Y. Sakurai: Appl. Radiat. Isot. **163** (2020) 109214. https://doi.org/10.1016/j.apradiso.2020.109214
2 D. M. Minsky, A. A. Valda, A. J. Kreiner, S. Green, C. Wojnecki, and Z. Ghani: Appl. Radiat. Isot. **69** (2011) 1858. https://doi.org/10.1016/j.apradiso.2011.01.030
3 A. Caracciolo, D. Di Vita, T. Ferri, M. Carminati, N. Protti, S. Altieri, F. Camera, and C. Fiorini: Nucl. Instrum. Methods Phys. Res., Sect. A **1048** (2023) 168019. https://doi.org/10.1016/j.nima.2023.168019
4 I. Murata, S.Kusaka, K. Minami, N. Saraue, S. Tamaki, I. Kato, and F. Sato: Appl. Radiat. Isot. **181** (2022) 110056. https://doi.org/10.1016/j.apradiso.2021.110056
5 T. Kobayashi, Y. Sakurai, and M. Ishikawa: Med. Phys. **27** (2000) 2124. https://doi.org/10.1118/1.1288243
6 I. Murata, T. Mukai, M. Ito, H. Miyamaru, and S. Yoshida: Prog. Nucl. Sci. Technol. **1** (2011) 267. https://doi.org/10.15669/pnst.1.267
7 M. Manabe, S. Nakamura, and I. Murata: Rep. Pract. Oncol. Radiother. **21** (2016) 102. https://doi.org/10.1016/j.rpor.2015.04.002
8 M. Manabe, F. Sato, and I. Murata: Appl. Radiat. Isot. **118** (2016) 389. https://doi.org/10.1016/j.apradiso.2015.11.003
9 M. Manabe, R. Ohya, N. Saraue, F. Sato, and I. Murata: J. Radiat. Prot. Res. **41** (2016) 328. https://doi.org/10.14407/jrpr.2016.41.4.328
10 B. Hales, T. Katabuchi, M. Igashira, K. Terada, N. Hayashizaki, and T. Kobayashi: Nucl. Instrum. Methods Phys. Res., Sect. A **875** (2017) 51. https://doi.org/10.1016/j.nima.2017.09.009
11 S. Fatemi, C. H. Gong, S. Bortolussi, C. Magni, I. Postuma, M. Bettelli, G. Benassi, N. Zambelli, A. Zappettini, X. B. Tang, S. Altieri, and N. Protti: Nucl. Instrum. Methods Phys. Res., Sect. A **936** (2019) 50. https://doi.org/10.1016/j.nima.2018.09.135
12 M. Sakai, S. Tamaki, I. Murata, R. K. Parajuli, A. Matsumura, N. Kubo, and M. Tashiro: Sci. Rep. **13** (2023) 22883. https://doi.org/10.1038/s41598-023-49955-9
13 K. Hitomi, T. Onodera, S.-Y. Kim, T. Shoji, and K. Ishii: Nucl. Instrum. Methods Phys. Res., Sect. A **747** (2014) 7. https://doi.org/10.1016/j.nima.2014.02.020
14 K. Hitomi, T. Shoji, and K. Ishii: J. Cryst. Growth **379** (2013) 93. https://doi.org/10.1016/j.jcrysgro.2013.03.002
15 T. Lee, H. Lee, and W. Lee: Nucl. Instrum. Methods Phys. Res., Sect. A **798** (2015) 135. https://doi.org/10.1016/j.nima.2015.07.038
16 M. Nogami, K. Watanabe, and K. Hitomi: Jpn. J. Appl. Phys. **63** (2024) 096002. https://doi.org/10.35848/1347-4065/ad7803
17 K. Hitomi, T. Shoji, and Y. Niizeki: Nucl. Instrum. Methods Phys. Res., Sect. A **585** (2008) 102. https://doi.org/10.1016/j.nima.2007.11.012
18 K. Hitomi, Y. Kikuchi, T. Shoji, and K. Ishii: IEEE Trans. Nucl. Sci. **56** (2009) 1859. https://doi.org/10.1109/TNS.2009.2013349
19 Z. He, G. F. Knoll, D. K. Wehe, R. Rojeski, C. H. Mastrangelo, M. Hammig, C. Barrett, and A. Uritani: Nucl. Instrum. Methods Phys. Res., Sect. A **380** (1996) 228. https://doi.org/10.1016/S0168-9002(96)00352-X
20 Z. He, G. F. Knoll, D. K. Wehe, and J. Miyamoto: Nucl. Instrum. Methods Phys. Res., Sect. A **388** (1997) 180. https://doi.org/10.1016/S0168-9002(97)00318-5